INSTITUTE OF PLASMA PHYSICS

NAGOYA UNIVERSITY

RESEARCH REPORT

NAGOYA, JAPAN

"Resonances of Radio Frequency Probe
in a Plasma"

Hiroyuki IKEZI
and Kazuo TAKAYAMA

IPPJ-48 March 1966

Further communication about this report is to be sent to the Research Information Center, Institute of Plasma Physics, Nagoya University, Nagoya, JAPAN.

Abstract

The RF probe experiment is carried out by the use of a low density plasma, and resonances of the probe impedance are studied. We observed two resonances in a frequency range between the sheath-plasma resonance and the plasma frequencies.

A mechanism of the additional resonances is discussed. It is shown that finite electron temperature introduces resonances in addition to the sheath-plasma resonance. Choosing some artificial density distributions in front of the probe, the frequency dependence of the resonances is explained qualitatively.

§ Introduction

In recent reports[1) 2)] on the resonance rectification probe developed by Takayama[3)] et al., there have been found two resonances. One of them is known as a sheath–plasma resonance[4)] by the comparison with a RF probe experiment[5)]. As to the other nigher frequency side resonance (second resonance), however, there is no theoretical explanation yet.

In earlier experiment, Tonks[6)] and Dattner[7)] found that a plasma column showed several resonances upon the incidence of microwave at the frequencies lower than the plasma frequency. Recently the theories on this phenomenon are proposed[8) 9)]. They have explained the experimental results by assuming that the plasma has a finite electron temperature and density gradient. Here, it is shown that the additional resonances of a probe could be explained by the same mechanism as that of the Tonks–Dattner resonances from following informations. The RF probe experiment is not different from the experiment by Tonks and Dattner except for the method of coupling between the plasma and the oscillator. As is shown in this report, the second resonance is observed in RF probe experiment. Moreover, we have found three resonances for strongly negative probe.

In this paper, we shall report the experiment which will show the characters of the additional resonances. The frequency dependence of the impedance is calculated with the idea along the same line of the theory for Tonks–Dattner resonance. The results are compared with the present experiment.

§ Experimental Arrangement and Method

In the figure 1(a), the low–pressure mercury–vapor discharge

tube used in the present experiment is shown schematically. Two plasma sources are placed at the opposite side of a spherical bottle. After the discharge in the plasma source, plasma diffuses into the bottle. The grids, which separates the source from the bottle, prevent the propagation of the fluctuation in the discharge region to the bottle. In order to obtain reproducible results, the vapor pressure depending on the temperature of a mercury reservoir was stabilized by a thermostat during several hours.

In this type of tube there produces a plasma of density 10^6/cc and of electron temperature 3000°K. Two disc probes of 30 mm diameter with a separation of 20 cm were inserted from both sides of the bottle. The plasma is very quiet, and only the shot noise and the thermal noise are detected by these probes[10].

With the circuit which is shown in Fig. 1(b), the resonance probe experiment (the resonance rectification of RF current by the probe) and the measurement of the RF current through the plasma between two electrodes, which are shown in Fig. (1 a) as P and Fig. (1 c) as E, are carried out. The signal from the RF oscillator (10 Kc to 50 Mc) is terminated at the probe 1 or one of the plates so as to produce constant voltage at the terminals, whose value is several ten milli volts. During the resonance probe measurement the DC probe current is recorded through the voltage at Y_1 or Y_2. The RF current through the plasma is recorded at Y_3. The signal applied to the diode is so small that the detector shows quadratic character.

Measurements were carried out by varying the frequency at fixed discharge currents. The probe current and the RF current through the plasma are plotted by an X – Y recorder. We did not measure separately the real and the imaginary parts of the admittance but the sum of the square of them.

§ Experimental Results

In order to check whether or not the rectified current by the probe and the RF current have the same resonant frequency, a measurement of both currents is carried out at the same discharge current. The typical characteristic curves of the rectified current of the exciting probe (p_1) and of the detecting probe (p_2), and that of RF current I_{rf} are plotted in Fig. 2. In this case, the frequencies of the first peaks (sheath–plasma resonance) and the second peaks are 9.2 ~ 9.5 Mc and 11.4 ~ 11.6 Mc respectively. The first resonant frequency of the exciting probe is slightly lower than that of the other two cases. This difference is due to their geometries and is inessential. From this figure, we see that the resonant frequencies of RF current are the same as those of the rectified current. Therefore, we conclude that the second resonances observed in those different two experiment are due to the same mechanism.

If the second resonance results from plasma wave, the resonant frequency must change with the electron density distribution, which is varied by the probe bias. The RF currents are plotted in Fig. 3 for extremely different probe biases and fixed discharge current. When the probe bias becomes strongly negative, the height of the main resonance peak is reduced and that of the second resonance peak is increased. We find also the third resonance peak. The resonant frequency and the height of the resonant peaks are shown in Fig. 4 as a function of probe bias V_p. When the probe bias increases, the resonant frequency slightly decreases for the main resonance and increases for the second and the third resonances. The height of the second peak is almost constant for strongly negative probe. When the electron current increases the second and third peaks disappear.

In the theory of the Tonks–Dattner resonance, the resonant frequency is a function of A/λ, where A is the thickness of a plasma and λ the Debye length. A similar parameter L/λ or d/λ also decides the resonant frequency in our calculation which is discussed in the following sections. Here L and d are the distance between two electrodes and the radius of electrodes respectively. The Debye length can be varied by changing the discharge current.

The resonant frequencies in the unit of the plasma frequency, are shown in Fig. 5. This data are obtained at the floating potential. The plasma frequency corresponding to the maximum density is obtained from the minimum RF current[4]. The electron temperature is measured by the Langmuir probe method. The resonant peak does not appear in the frequency region higher than the plasma frequency. For the case of disk probes, the lines which represent the ratios f/f_p of the resonant frequencies to the plasma frequency crosses the line $f/f_p = 1$. At the crossed point the resonant peak and the minimum current overlap each other like the curve shown in Fig. 3.

For the case of the outer plates, the retios f/f_p are much smaller than the case of the probes. This discrepancy is due to the difference of geometries of these electrodes. When the distance L is much larger than the radius d, the ratio f/f_p depends on d/λ, and when d is larger than L, f/f_p depends on L/λ. This fact will be discussed in the following sections.

When we plot Fig. 5, the plasma frequency is obtained from the minimum RF current. As we see in the next section, this method is correct even for the finite temperature plasma. In fact, the minimum RF current gives experimentally the same frequency for different two geometries within the error of experiment. The frequency which gives the minimum RF current is, however, very sensitive to the stray capacity of the circuit. From this reason, the RF current which is

measured at the exciting probe side does not give rise to the correct result.

§ Derivation of Impedance

In this section, we derive the impedance of the hot and non-uniform plasma between two electrodes and show the results of numerical calculations. We shall use the hydrodynamical equations for an electron gas, and adopt the quasi-static approximation, for the dimension of our plasma (~ 30 cm) is sufficiently smaller than the wave length in vacuum (several ten meters).

$$m\,(d\vec{v}/dt + \nu\,\vec{v}) = e\vec{E} - kTn^{-1}\,\nabla n, \tag{1}$$

$$\partial n/\partial t + \nabla\cdot(nv) = 0, \tag{2}$$

$$\nabla\cdot\vec{E} = 4\pi e\,(n - n_i). \tag{3}$$

Here, $\vec{v}$ is the macroscopic electron velocity, n the electron density, n_i the ion density, $\vec{E}$ the electric field, ν the collision frequency, and e and m the charge and the mass of an electron respectively. For simplicity, we have assumed the electron temperature T = const. We now replace the variables in (1) – (3) (denote by F symbolically) by $F_0\,(x) + F_1\,(x)\exp(i\omega t)$, where the index 1 is to stand for the perturbed quantity. We consider only a strongly negative probe, thus $\vec{v}_0 = 0$. This assumption will be discussed after the equation for the current is derived. Equations (1), (2) and (3) now become

$$\vec{E}_0 = (kT/e)\,\nabla n_0/n_0, \tag{4}$$

$$\nabla\cdot\vec{E}_0 = 4\pi e\,(n_0 - n_i), \tag{5}$$

$$-\omega\,(\omega - i\nu)\,\vec{j}_1 = \omega_p^2\,(\vec{I}_1 - \vec{j}_1) - v_T^2\,(\nabla n_0/n_0)\,\nabla\cdot\vec{j}_1 + v_T^2\,\nabla\,(\nabla\cdot\vec{j}_1), \tag{6}$$

where, $\omega_p^2(x) = 4\pi e^2 n_o(x)/m$, $v_T^2 = kT/m$, $\vec{j}_1 = e n_o \vec{v}_1$ and $\vec{v}_o = 0$. (7)

Here, I_1 is the total current density defined by

$$I_1 = j_1 + (i\omega/4\pi) E_1. \tag{8}$$

The equation (4) shows the balance between the pressure and the electric force which results from space charge represented by (5).

In the following we shall consider a plasma between parallel-plates for simplicity. Two plates are placed at the position $x = \pm L/2$, and the plasma density is assumed be spatially uniform in y and z directions. We assume $\partial/\partial y = \partial/\partial z = 0$ in Eq. (6), then the equations (4) to (6) are reduced to

$$J'' - (g'/g) J' + (L/\lambda)^2 (\varepsilon - g) J = -g(L/\lambda)^2 \tag{9}$$

and

$$J + (i\omega/4\pi) E_1/I_1 = 1, \tag{10}$$

where $g(u) = \omega_p^2/\omega_{po}^2$, $\varepsilon = \omega(\omega - i\nu)/\omega_{po}^2$, $u = x/L$ and

$$J = j_1/I_1. \tag{11}$$

Here, J' and J'' are the first and the second derivatives of J with respect to u, and all quantities E, I and J should be read as x − components of those vectors. If the total current equals zero and the plasma is uniform, we obtain from (9) the familiar dispersion relation: $\omega(\omega - i\nu) = \omega_p^2 + k^2 v_T^2$. We obtain the impedance Z per unit area from the solution of (9) and the expression (10)

$$Z = L/I_1 \int_{-1/2}^{1/2} E_1 \, du = 4\pi L/i\omega \left(1 - \int_{-1/2}^{1/2} J du\right). \tag{12}$$

The first term of R.H.S. of the expression (12) represents the capasitive component of parallel plates and the second term of it the reactive component due to the plasma current.

Before solving the differential equation (9), we should have some consideration about the assumption $\vec{v}_o = 0$. This assumption

introduces that the probe is biased by $-\infty$. Therefore, g(u) must be zero at the boundaries ($u = \pm 1/2$). This condition leads $\vec{E}_o = \pm\infty$ at those places, because $\vec{E}_o$ is proportional to g'/g (see Eq. (4)). Conversely, it is obvious that $\vec{E}_o = \pm \infty$ gives rise to infinite negative bias. In the case of $\vec{v}_o = 0$, J must be zero, because g is zero. This gives the complete boundary condition for Eq. (9). When probe bias is finite as in the experiment, g ($\pm 1/2$) is not zero, and $\vec{v}_o$ is finite. Such g (u) introduces ambiguities on the boundary condition, and the wave equation becomes very complicated. When the probe is biased strongly negative, an assumption of $\vec{v}_o = 0$ is, however, a good approximation except for just in front of the wall. Thus we set g ($\pm 1/2$) = δ and assume J ($\pm 1/2$) = 0.

In order to compare the results of calculation with experiments we must choose a realistic density variation. Itatani[11] calculated the density profile for one-dimensional case. Here we approximate his density profile by a sinusoidal form and assume g (u) as an even function. One of the examples of the calculated density profile and our g(u) are plotted in Fig. (6).

Because of the symmetry of the plasma, the driven part of the current in the plasma is an even function of position. In this way we miss certain natural oscillation modes driven by statistical fluctuation having odd symmetry. For a small amplitude oscillation, these odd modes are uncoupled with the even ones and do not contribute to the impedance.

The equation (9) is solved by an electronic computer by the use of the boundary condition J ($\pm 1/2$) = 0. One of the result is plotted in Fig. (6) and Fig. (7). In this case, when ω/ω_{po} is smaller than 0.7, the current J increases with ω/ω_{po} at every point. Therefore the integral in Eq. (12) is monotonically increasing function of ω/ω_{po}. If the collision is neglected, the integral

becomes unity and the impedance becomes zero at some value of ω/ω_{po} smaller than 0.7. This corresponds to the sheath-plasma resonance. When ω/ω_{po} is greater than 0.7, current J oscillates spatially. This oscillation corresponds to a standing plasma wave in the sheath. Therefore the integral oscillates with an increase of ω/ω_{po}, and values of ω/ω_{po} at which the integral is unity give a series of resonances. Inserting the solution of Eq. (9) into Eq. (12) the impedance is calculated. The result is shown in Fig. (8). For convenience, we have introduced the admittance Y which is inverse of the impedance. In the case shown Figs. (6), (7) and (8) we find only one additional resonance. But, as seen in Fig. (9c), two additional resonances appear, when the thickness of the sheath is increased. We shall find more resonant peaks, when the distance between two plates and the thickness of the sheath are increased. This result is consistent with experiments, which are shown in Fig. (3).

The dependence of the resonant frequency on the thickness of the sheath is shown in Fig. (9). As it is expected, the resonant frequency becomes lower, when the sheath expands. For the expansion of the sheath results in the decrease of the electron density in the sheath, therefore the current J changes its sign in the sheath for lower frequency. On the other hand, the frequency of the sheath-plasma resonance becomes slightly higher with the expansion of the sheath. This character may be explained by simple consideration[4)12)*)]. These results on resonant frequency agree with the experiments which is shown in Fig. (4). In the present calculation, however, the dependence of the resonant frequency on the thickness of the sheath

---

*) If the temperature goes to zero, λ becomes zero. The equation (9) is simplified as $J = (1-\varepsilon)^{-1}$ for an uniform plasma. If the plasma has sharp boundary and its thickness is Λ ($< L$). The impedance is $(4\pi L/i\omega)\left[1 - (\Lambda/L) - \varepsilon\right]/(1-\varepsilon)$. If $\nu = 0$. the resonant frequency is $\omega_p\left[1 \mp (\Lambda/L)\right]^{1/2}$, and anti-resonance occurs at ω_p.

is not remarkable, but on the ratio L/λ which may be seen in Figs. (5) and (9). As seen in Fig. (9), $|Y|$ always takes minimum value at $\omega/\omega_{po} = 1$ except for the case in which the additional resonance appeares at $\omega/\omega_{po} = 1$.

In order to discuss the geometrical factor, we consider a couple of concentric spheres. The radii of the inner and the outer sphere are a_0 and a_1 respectively. The space between two spheres is filled with a plasma. Here, we write down the equations in poler coordinate. In the representation of the impedance, only radial component of the plasma current is sufficient. If we assume that the plasma density varies only along radial direction, that is $\partial/\partial\theta = \partial/\partial\varphi = 0$, Eq. (6) is reduced to

$$\frac{d}{d\rho}\left[\frac{1}{\rho^2}\frac{d(\rho^2 J)}{d\rho}\right] - \left(\frac{dg}{d\rho}/g\right)\frac{1}{\rho^2}\frac{d(\rho^2 J)}{d\rho} + \left(\frac{a_0}{\lambda}\right)^2(\epsilon - g)J = -\left(\frac{a_0}{\lambda}\right)^2 g, \tag{13}$$

and

$$z = \frac{1}{i\omega a_0}\left[1 - \frac{a_0}{a_1} - \int_1^{a_1/a_0} J\, d\rho\right], \tag{14}$$

where

$$\rho = r/a_0, \quad J = j_{1r}/I_{10} \quad \text{and} \quad I_1 = I_{10}/\rho. \tag{15}$$

Here, we have used that $\vec{I}$ has only radial component. When the ratio a_1/a_0 is much greater than unity, the impedance may be written as

$$z = \frac{1}{i\omega a_0}\left[1 - \int_1^{\infty} J\, d\rho\right] \tag{16}$$

because J is proportional to $1/\rho^2$ at distant point. In this case the outer sphere only plays a role of a reflector for the waves.

The equation (13) does not include the characteristic length except for the coefficients as in the case of Eq. (9). Therefore, we can conclude from Eq. (12) and Eq. (16) that the resonant frequencies are a function of L/λ for the plane electrodes and are a function

of a_o/λ for the spherical ones. This conclusion explains the difference of resonant frequencies on two experimental conditions which are shown in Fig. (5). In the experiment, we have used the plane probes with the radii smaller than both the thickness of the sheath and the separation of probes. Therefore it may be considered that the probes behave as the spherical dumbell. In this case the resonant frequency is independent from L to the first order, but depends on a/λ, since $L \gg d$. On the other hand, since the diameter of the plates out side the sphere are greater than the effective L, its geometry may be approximated by one-dimensional parallel plates. Therefore the one dimensional calculation, which we have carried out, should be adequate to explain the experimental results. As a matter of fact, an extremely good agreement between them is seen in Fig. (5).

Lastly, we should mention about the validity of the assumption: $J = 0$ at $u = \pm 1/2$. This assumption states that the plasma wave reflect perfectly at the wall. When the probe potential approaches the plasma potential, this assumption does not hold any longer. As we see in Fig. (4), the height of additional peak decreases rapidly near the plasma potential before the resonant frequency does not shift largely. This may be due to that the wall absorbes the plasma wave. Even though the travelling wave exsists, it does not affect the impedance, because the phase angle between the oscillating component of J and RF voltage depends on time.

§ Discussion

From the following results, we arrive at a conclusion that the additional resonant peaks should result from the standing plasma wave in a sheath.

a) Two additional resonances were observed.

b) The resonant frequency is always lower than the plasma frequency, and the ratio f/f_p depends on λ and the probe bias.

c) The frequency which corresponds to the minimum RF current does not depend on geometry.

d) The frequency characteristic curve of the impedance derived from the theory is consistent qualitatively with the experimental results from a) to c). Though we may explain the resonances qualitatively, there are some problems remained to clear up. Firstly the geometry of the electrodes is not ideal in our experiment, so that the end effect should be eliminated. Secondly, the electron density distribution in the sheath should be determined experimentally in order to say something more quantitatively about the resonances. Thirdly, the boundary condition in our calculation is not perfect which should be examined more carefully. Lastly, in the present theory we must know the amplitude of the plasma current in order to predict the resonant frequency. It is the only difficulty for the quantitative agreements on the present resonances which was free for the theory dealing with the natural modes that is the Tonks-Dattner resonance. Therefore, the loss rate of energy must be important. Here, we have considered only collision damping and not considered Landau damping and the wall-loss. As we see in Fig. (4), the second peak disappears, when the probe bias is near the plasma potential. This disappearance of the peak must be due to the wall-loss. In fact, near the plasma potential electrons flow to the probe which result in the wall-loss of the plasma wave.

§ Acknowledgement

The authers wish to express their appreciation to Dr. R. Itatani and Dr. R. Sugihara for their helpful discussions. They are grateful to Dr. A. Ouchi for his numerical calculations on the electronic computer.

Reference

1) H. M. Mayer: MPI-PA 25/64, Max-planck Institute für Physik und Astrophysik München (1964)

2) T. Dote and T. Ichimiya: J. Appl. Phys. 36 1866 (1965)

3) K. Takayama et al.: Phys. Rev. Letters 5 238 (1960)

4) Levitskii: Soviet Physics-Technical Physics 8 319 (1963)

5) J. Uramoto et al.: IPPJ-19, Institute of Plasma Physics Nagoya Univ. (1963)

6) L. Tonks: Phys. Rev. 37 1458 (1931)

7) A. Dattner: Ericsson Tech. 13 309 (1957): Phys. Rev. Letters, 10 205 (1963)

8) Weissglass: Phys. Rev. Letters 10 206 (1963)

9) F. C. Hoh: Phys. Rev. 133 A 1016 (1964)

10) To be published

11) Private Communication from Itatani: He calculated zeroth order equation and obtained density distribution.

12) F. W. Crawford and R. S. Harp: J. Geophys. Res. 70 587 (1965)

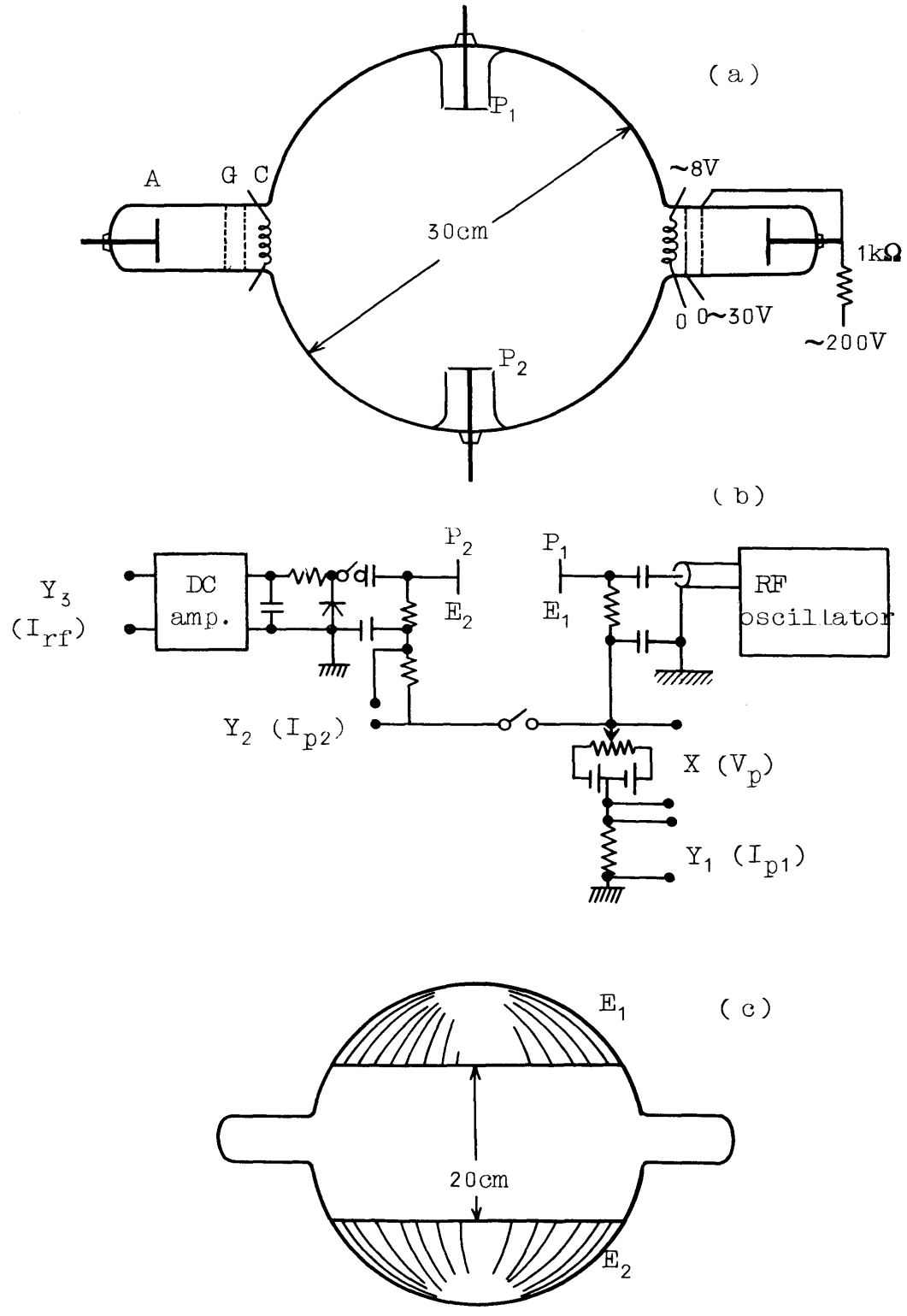

Fig. 1. (a) A sketh of the discharge tube. Here, A is the anode, G is the grid, C is the oxide coated cathode, and P_1 and P_2 are the probes.
(b) A circuit for measurement of the DC probe current and the RF current through a plasma.
(c) A sketch of outer alminium plates.

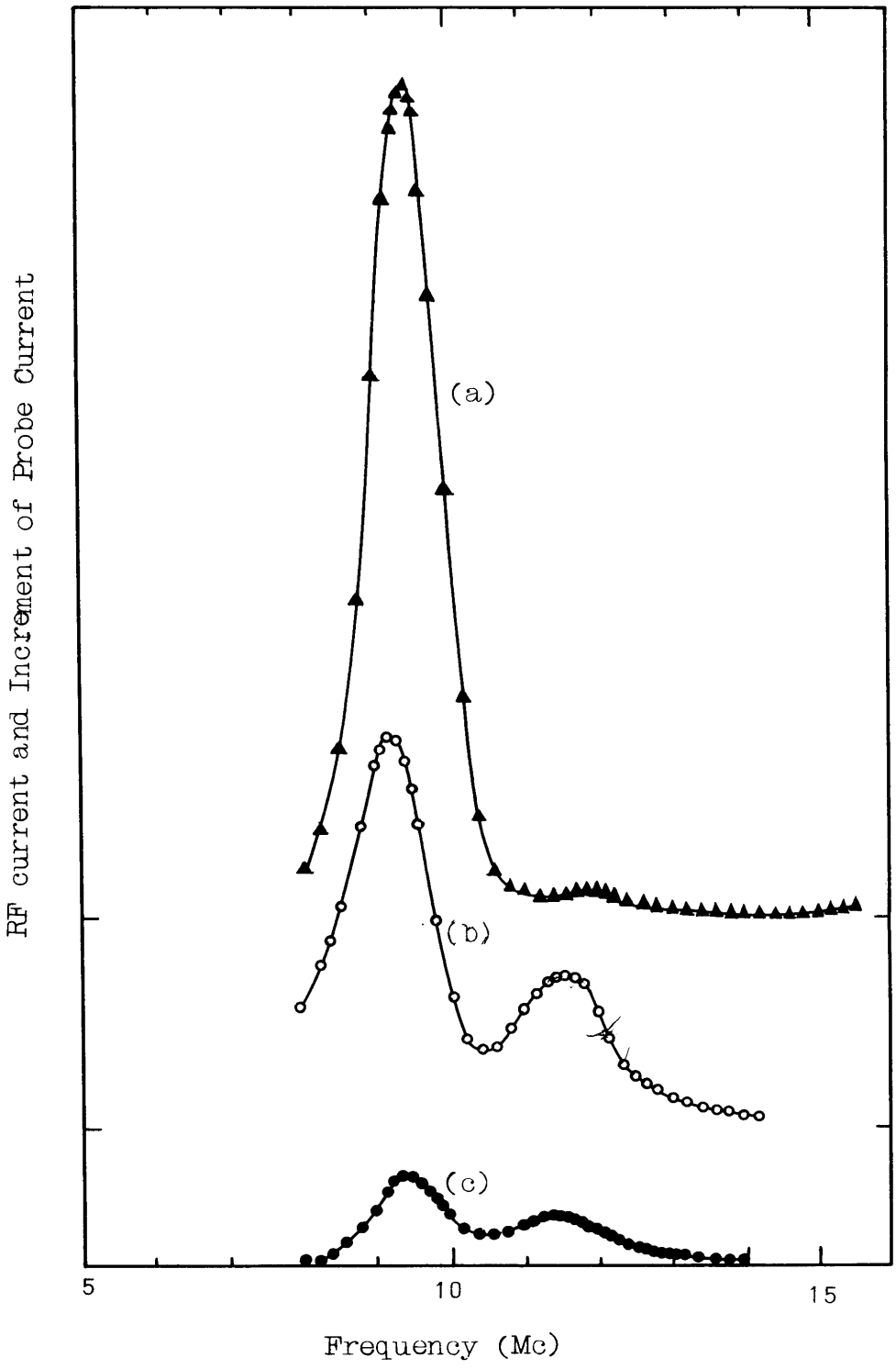

Fig. 2. Frequency characteristic curve of the RF current and the increment of the DC probe current, when the probes are at the floating potential and the RF voltage is constant. The curves b and c show the DC current at P_1 and P_2 respectively, and (a) shows the RF current.

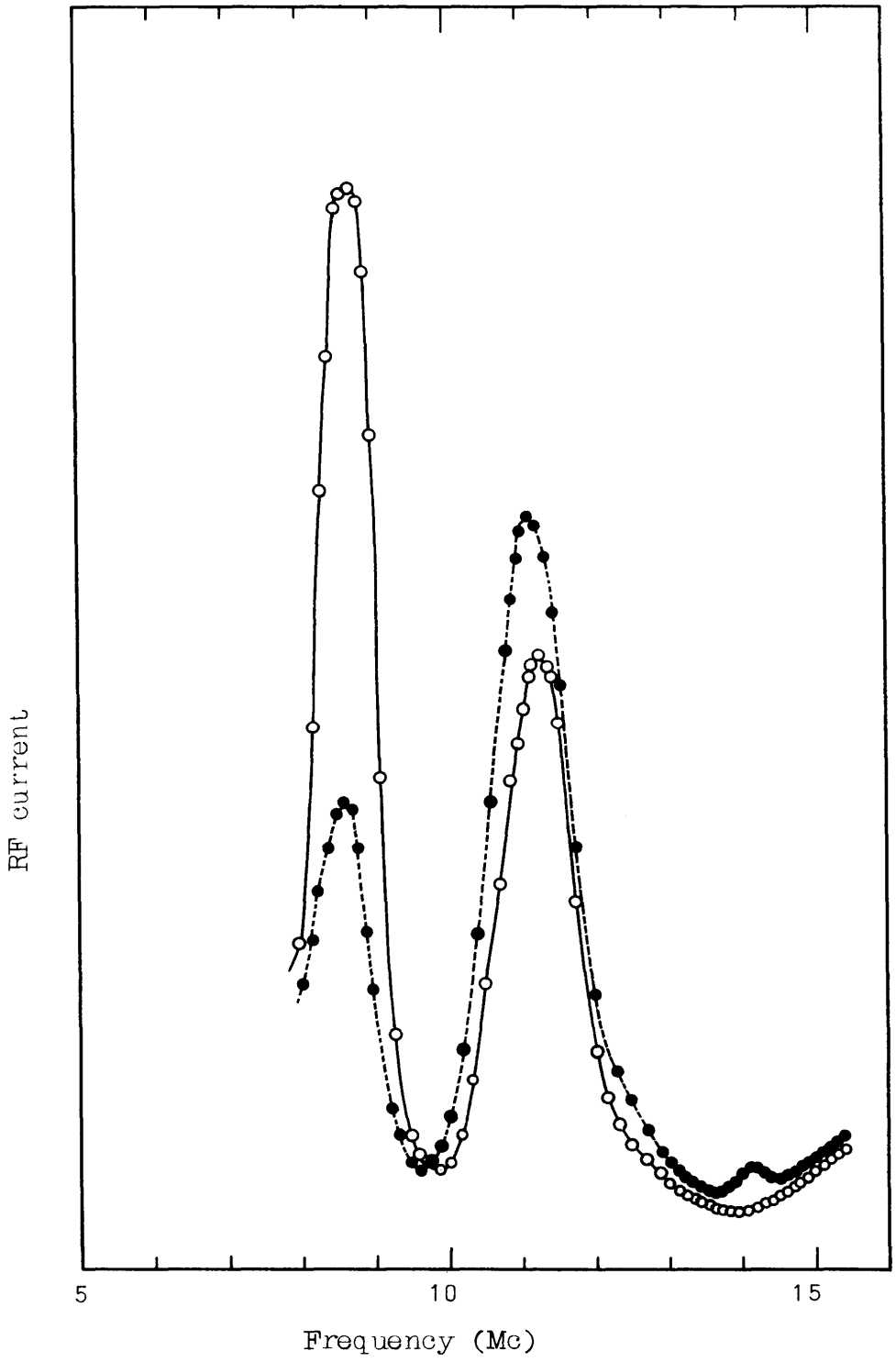

Fig. 3. Frequency characteristic curve of the RF current. The solid and dotted curves correspond to $V_p - V_s = -10$ volts and -20 volts respectively, where V_p and V_s are the probe bias and the space potential respectively.

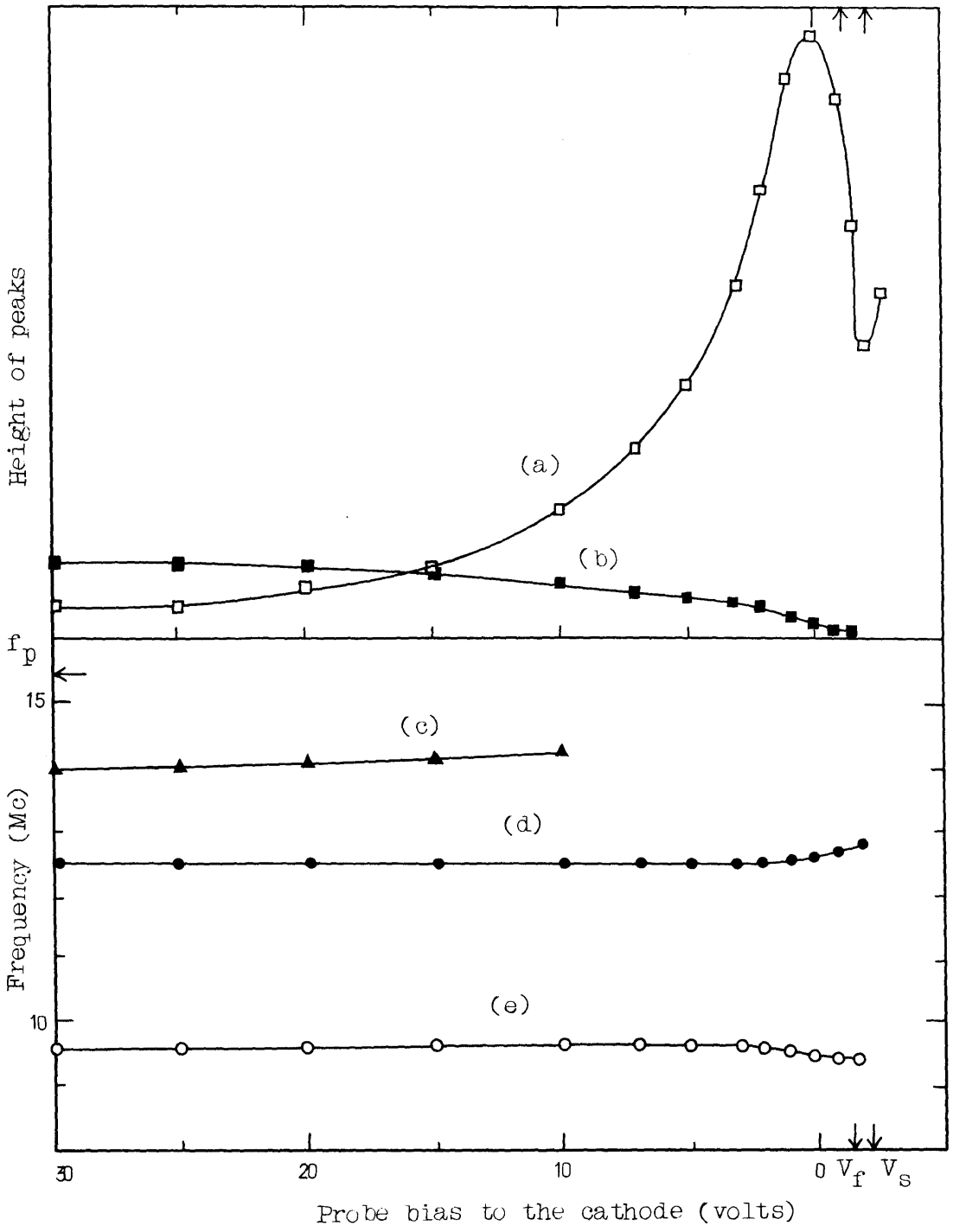

Fig. 4. The heights of resonant peaks and the resonant frequencies as a function of the probe bias. Curve (a) and (e) are correspond to the sheath-plasma resonance, (b), (d) and (c) are to the second and the third resonances respectively.

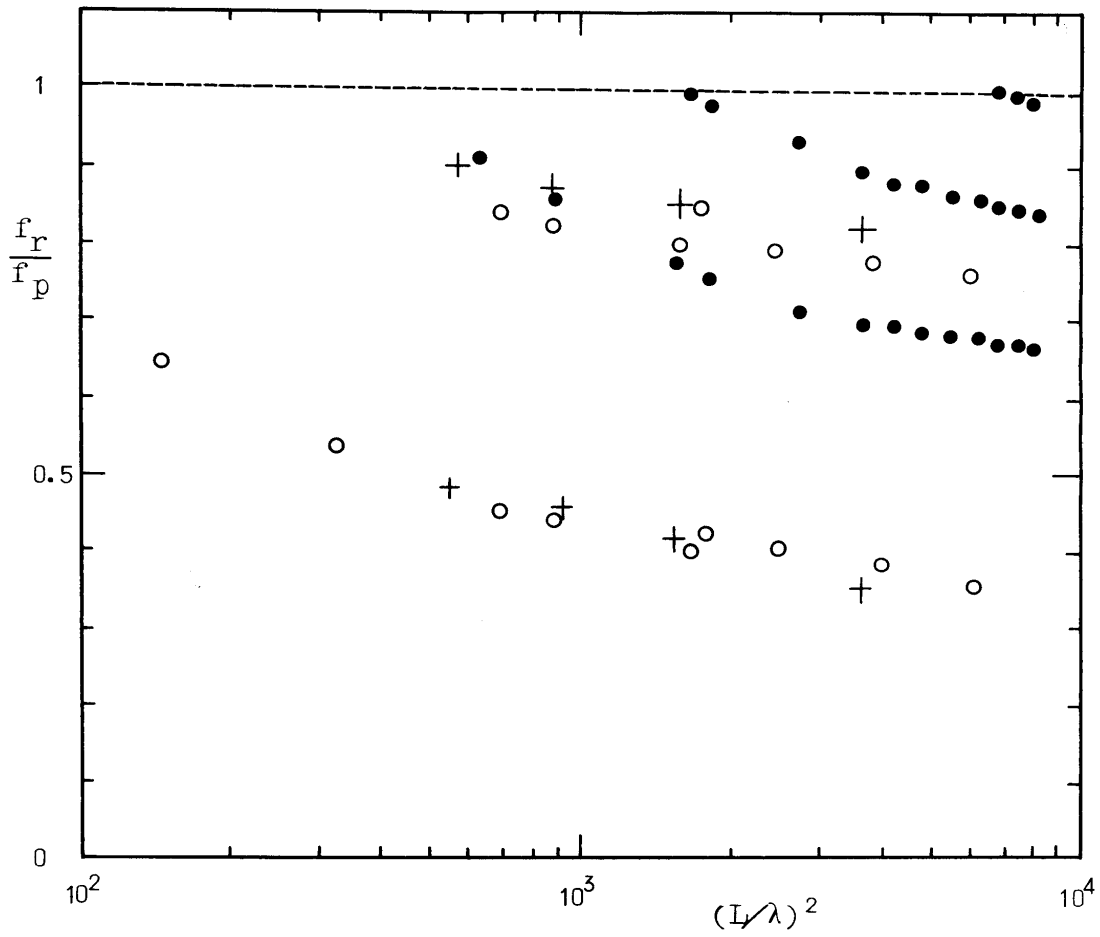

Fig. 5. The ratio of the resonant frequency f_r to the plasma frequency are shown as a function of $(L/\lambda)^2$.

● : The probes at floating potential

O : The outer plates

\+ : By the theory. The density profile of the sheath is the same as that which is shown in Fig. 6.

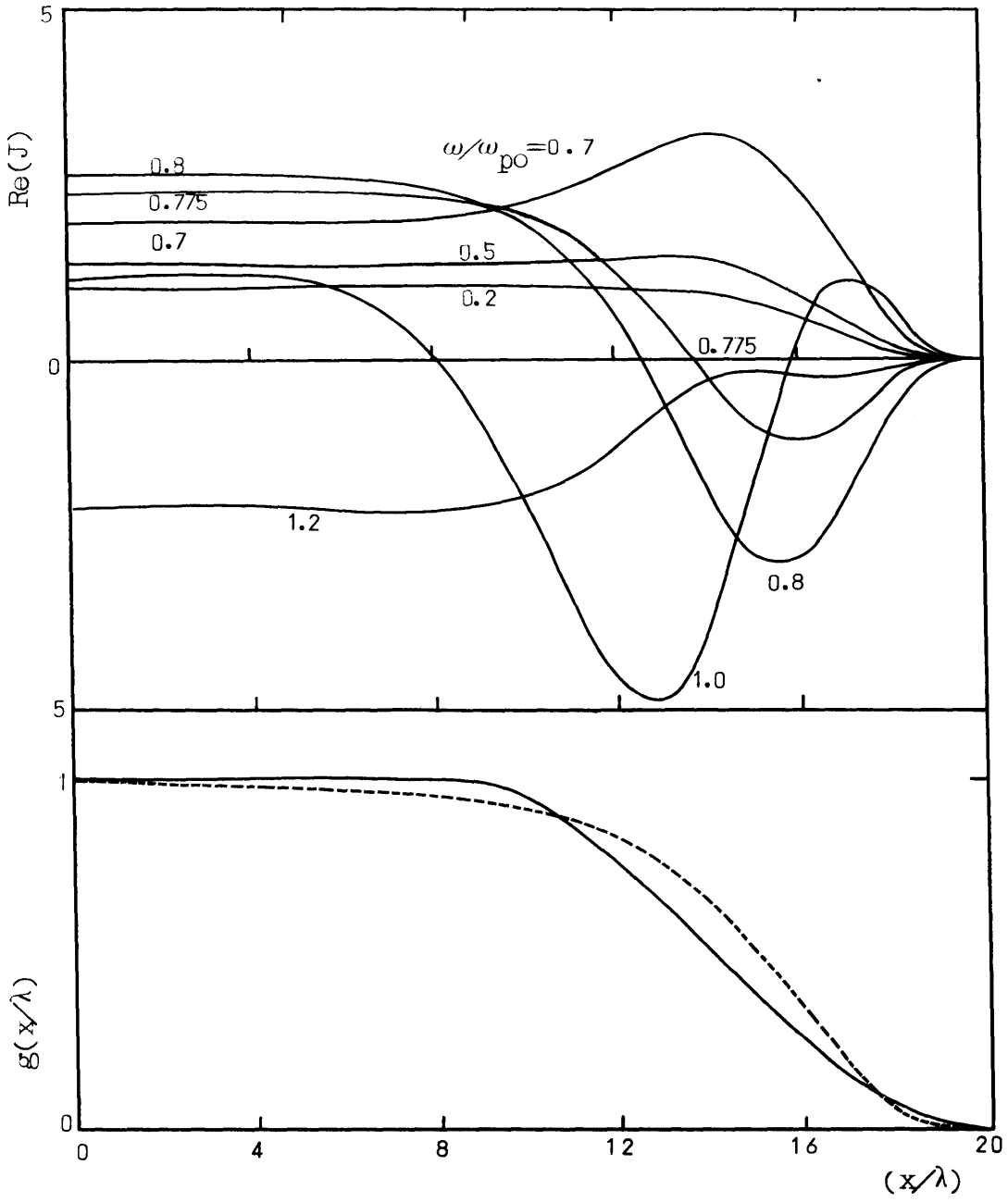

Fig. 6. The normalized electron density g and the real part of the normalized current J as a function of x/λ. The dotted curve is calculated by Itatani for the case in which the probe electron current is 10^{-3} times the electron satulation current. $\nu/\omega_{po} = 0.1$.

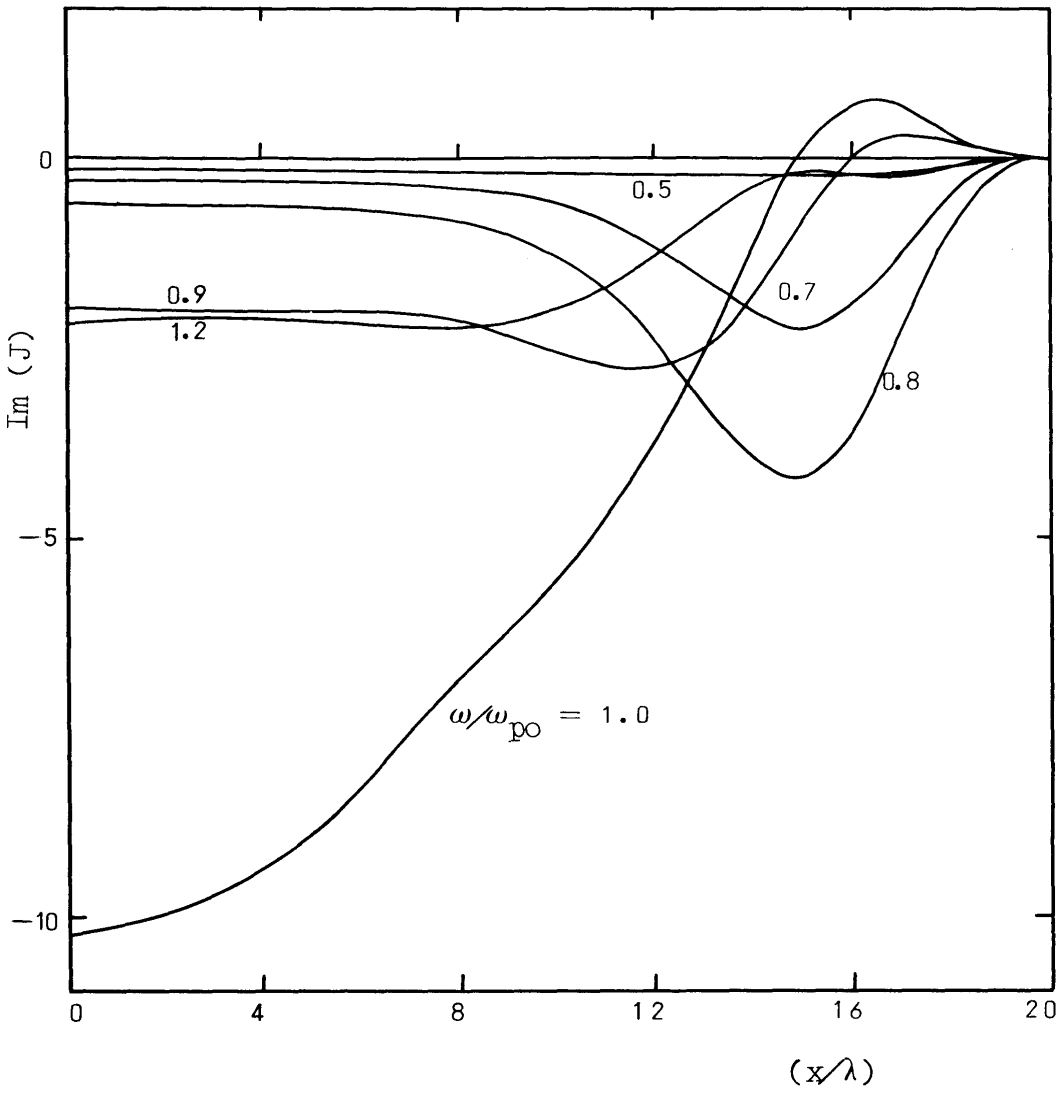

Fig. 7. The imaginary part of J. The density profile g is the same as that in Fig. 6.

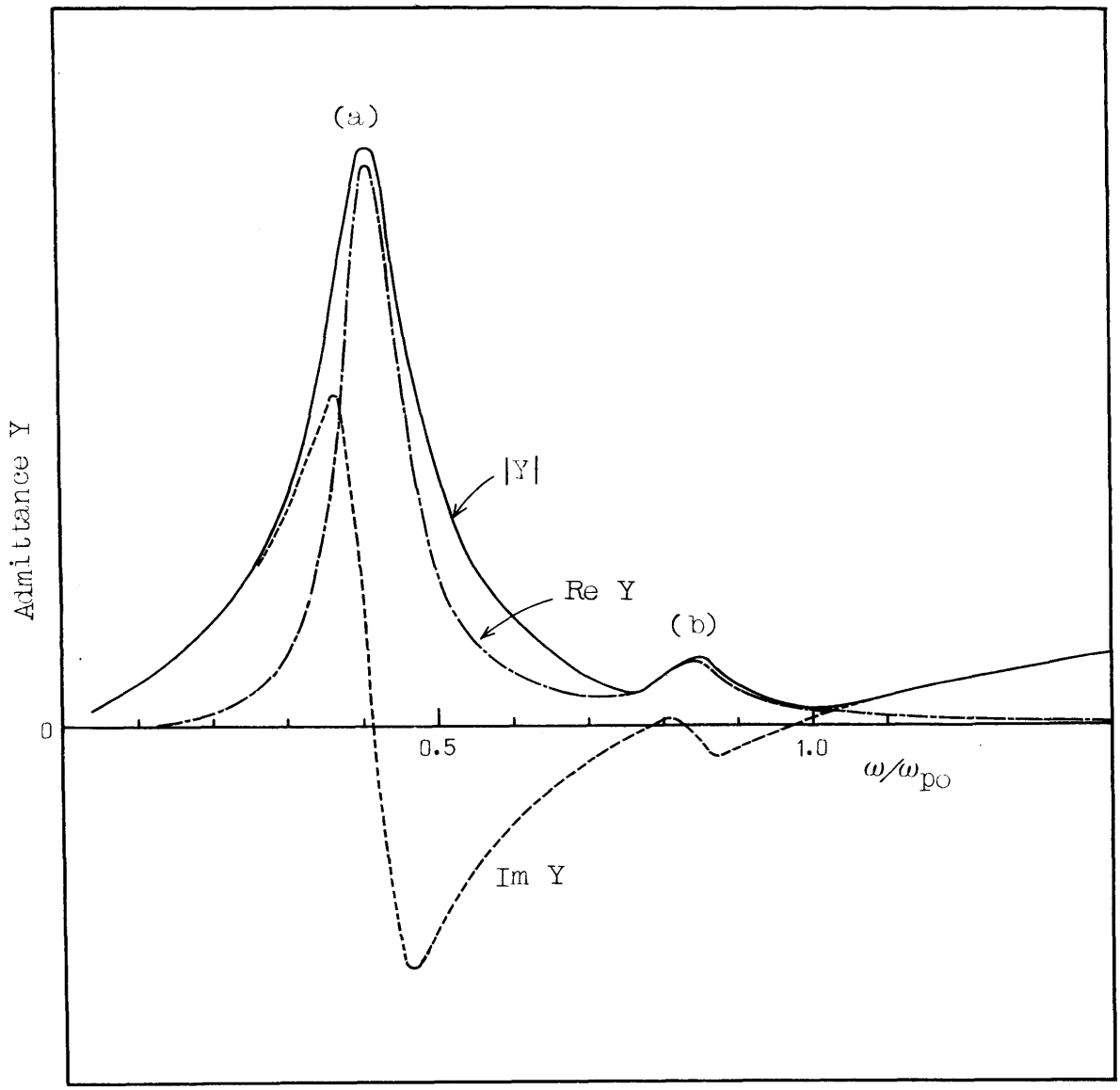

Fig. 8. The admittance as a function of ω/ω_{po}. Here, $\nu/\omega_{po} = 0.1$, and g is the same as that in Fig. 6. The peak (a) and (b) are the sheath-plasma resonance and additional resonance respectively.

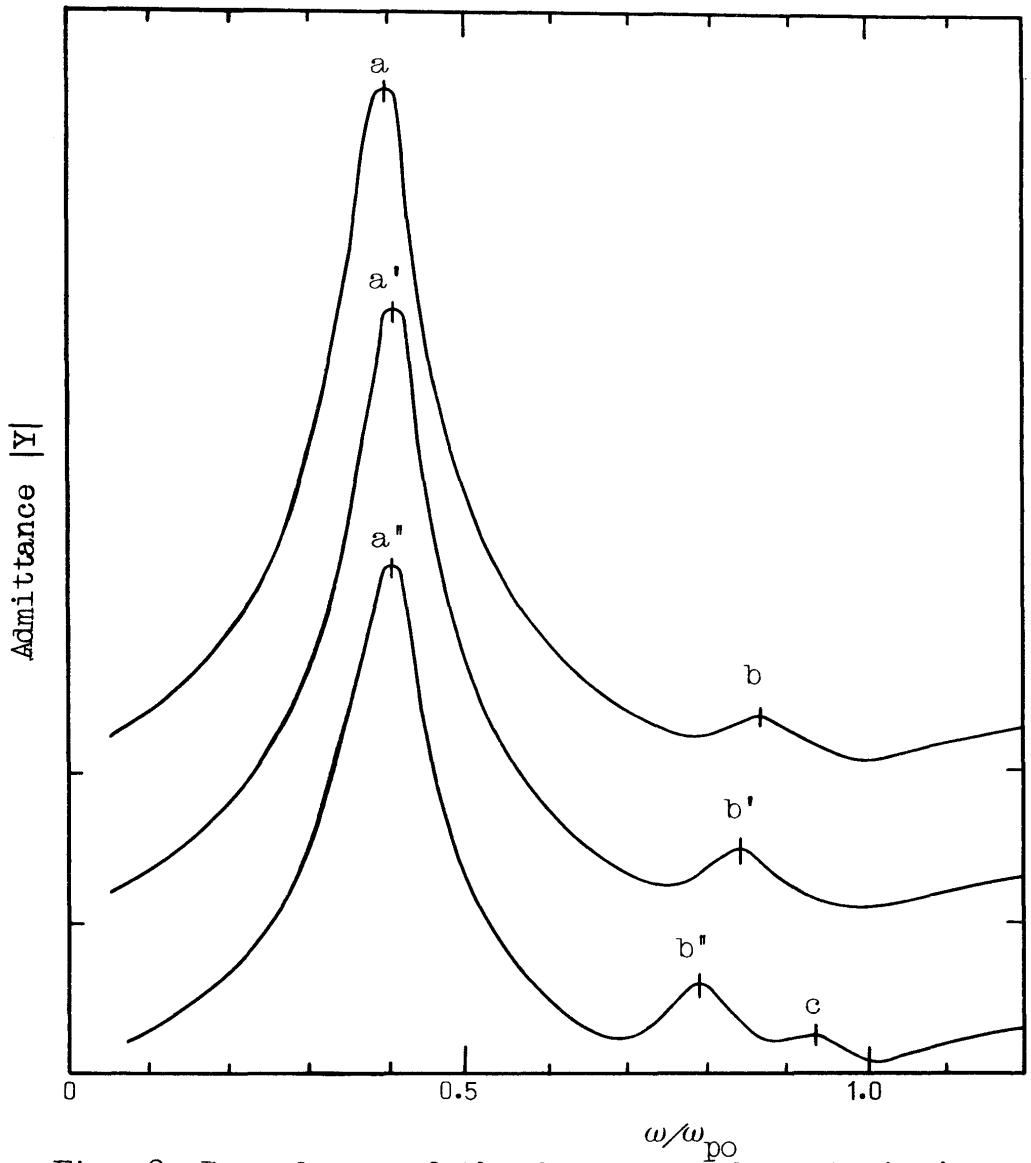

Fig. 9. Dependence of the frequency characteristics of the admittance on g.

$$\text{a b:g} = \begin{cases} 1 & , \ |x/\lambda| \leq 10 \\ \frac{1}{2.01}\left[1+\cos\left\{\frac{\pi}{10}\left(\frac{x}{\lambda}-10\right)\right\}+10^{-2}\right], & 20 \geq x/\lambda > 10 \\ \frac{1}{2.01}\left[1+\cos\left\{\frac{\pi}{10}\left(\frac{x}{\lambda}+10\right)\right\}+10^{-2}\right], & -20 \leq x/\lambda < -10 \end{cases}$$

$$\text{a' b':g} = \begin{cases} 1 & , \ |x/\lambda| \leq 8 \\ \frac{1}{2.001}\left[1+\cos\left\{\frac{\pi}{12}\left(\frac{x}{\lambda}-8\right)\right\}+10^{-3}\right], & 20 \geq x/\lambda > 8 \\ \frac{1}{2.001}\left[1+\cos\left\{\frac{\pi}{12}\left(\frac{x}{\lambda}+8\right)\right\}+10^{-3}\right], & -20 \leq x/\lambda < -10 \end{cases}$$

$$\text{a" b":g} = \begin{cases} 1 & , \ |x/\lambda| \leq 6 \\ \frac{1}{2.0001}\left[1+\cos\left\{\frac{\pi}{14}\left(\frac{x}{\lambda}-6\right)\right\}+10^{-4}\right], & 20 \geq x/\lambda > 6 \\ \frac{1}{2.0001}\left[1+\cos\left\{\frac{\pi}{14}\left(\frac{x}{\lambda}+6\right)\right\}+10^{-4}\right], & -20 \leq x/\lambda < 6 \end{cases}$$